Microscale Rheology of a Soft Glassy Material Close to Yielding

Pierre Jop,[1] Vincent Mansard,[1] Pinaki Chaudhuri,[2] Lydéric Bocquet,[2] and Annie Colin[1]

[1]*Université Bordeaux 1, Rhodia Laboratoire du Futur, Unité mixte Rhodia-CNRS, Université Bordeaux I, UMR 5258, Bordeaux, France*

[2]*Laboratoire PMCN, Université Lyon 1, UMR CNRS 5586, 69622 Villeurbanne, France*

(Received 9 September 2011; revised manuscript received 17 February 2012; published 3 April 2012)

Using confocal microscopy, we study the flow of a model soft glassy material: a concentrated emulsion. We demonstrate the micro-macro link between *in situ* measured movements of droplets during the flow and the macroscopic rheological response of a concentrated emulsion, in the form of scaling relationships connecting the rheological "fluidity" with local standard deviation of the strain-rate tensor. Furthermore, we measure correlations between these local fluctuations, thereby extracting a correlation length which increases while approaching the yielding transition, in accordance with recent theoretical predictions.

DOI: 10.1103/PhysRevLett.108.148301 PACS numbers: 47.57.Qk, 83.80.Ab

Amorphous materials are abundant in nature and also of great significance in industrial applications [1]. They only flow on applying an external stress exceeding the yield stress [2,3]. At this stage, a global picture describing the mechanisms at the origin of the flow starts to emerge [4,5]. In these jammed systems, flow occurs through a succession of elastic deformations and local irreversible plastic rearrangements associated with a microscopic yield stress [6–9]. The number of plastic rearrangements by unit time measures the fluidization of the system and increases as a function of the local applied shear stress. More strikingly, it is expected to exhibit nonlocality, and the rate of events depends upon the behavior of the neighborhood of a given zone—the rate is higher in the vicinity of an active zone, as compared to its value near a quieter one [8,10]. This cooperative behavior is due to the nonlocal elastic relaxation of the local shear stress after a plastic event, which induces an increase of the local stress in a zone close to an event [8,10]. Using such a model [8], some anomalous rheological behavior observed in the microfluidic flow of emulsions [5] could be explained and a correlation length could also be extracted by fitting the measured velocity profiles, evidencing the cooperative nature of flow. At this stage, what is missing is direct evidence of the link between the rheological *fluidity* of the system—here defined as the inverse viscosity, i.e., the ratio of shear rate to stress—and the locally occurring dynamical fluctuations that reflect the number of plastic events by unit time.

In this Letter, using dynamic confocal microscopy, we zoom down to the microscopic length scales to study the link between macroscopic rheology and local dynamical fluctuations in soft glassy systems. We focus, in particular, on the flow behavior of highly jammed systems when approaching the yielding threshold from above—i.e., at finite shear rates above the quasistatic regime. We demonstrate that there exists a scaling relationship between the fluidity and local strain-rate fluctuations. We quantify the correlations among the locally occurring fluctuations and we measure a corresponding correlation length which is measured to increase with decreasing strain rates.

Our experimental system is a concentrated, optically transparent emulsion of silicone oil droplets (polydimethyl siloxane of viscosity 1000 Pa · s) in a mixture of 50% water, 50% glycerol, surfactant (tetradecyl ammonium bromide), and rhodamine. The viscosity of the continuous phase is 10^{-2} Pa · s. The surface tension between oil and the continuous phase is 8 mN/m. The surfactant concentration within the aqueous phase is set to 1% in weight in order to ensure a good stability of the emulsion. It is high enough to prevent coalescence and low enough to avoid flocculation by depletion force, so that the emulsion is nonadhesive. The mean radius of the emulsion defined as $R_{32} = \frac{\langle R^3 \rangle}{\langle R^2 \rangle}$ is 7.5 μm. The size distribution is log normal, and the standard deviation is $\Delta R_{32}/R_{32} = 0.50$. The emulsion is polydisperse, which avoids crystallization in the bulk and near the surfaces. The volume fraction of the emulsion is $\phi \sim 0.75$, well above the jamming volume fraction $\phi_J \sim 0.65$. The macroscopic flow curves are determined by measurements in a rough cone-plate rheometer. It is well-described by a Herschel-Bulkley law $\sigma = \Sigma_c[1 + (\tau\dot{\gamma})^n]$, with the values $\Sigma_c = 31$ Pa, $n = 0.5$, and $\tau = 1/\dot{\gamma}_c = 2.5$ s. Neither aging nor dependence of the rheology on the flow history were evidenced.

We study the flow of emulsions in a homemade glass microdevice (Fig. 1), with a rectangular cross section (height $h = 1$ mm, width $w = 225$ μm, and length $L = 57.5$ mm). This is made by gluing two glass slides (1 mm thick) to a bottom glass slide with an optical adhesive (NOA 81, Norland Products) to form a straight channel of controlled width $w = 225$ μm [11]. The confining surfaces are rough, with a characteristic length scale, typically in the range of 1 μm. The flow is then controlled by applying a given pressure drop between the access holes. Rhodamine is added to the emulsion, which allows us to visualize the droplets using a confocal microscope (Zeiss LSM 5 Live) with an objective 40 ×

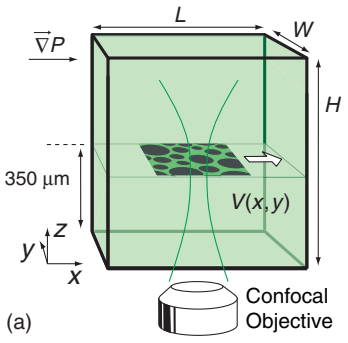

FIG. 1 (color online). Schematic diagram of the experimental device.

(confocal volume of 1.4 μm^3). From the recorded images, both the average velocity field and the local instantaneous strain rate are measured. To this end, images of the flow in the velocity (x direction) and in the gradient velocity plane (y direction) are taken line by line. The velocity direction and the scan direction are perpendicular. In those conditions, the delay time between two frames is 600 times higher than the scan time of one line, allowing a perfect determination of the displacements. The delay time between two frames varies between 0.2 to 0.016 s. The map of local displacement between two frames $(e_x(x, y, t), e_y(x, y, t))$ is calculated on a square grid with a mesh size of 3.5 μm. The intensity cross correlation for consecutive images is calculated for variable translations dx and dy along the flow (MATLAB procedure). The maximum of the intensity correlation (plus the shift) corresponds to a local displacement between the two frames $(e_x(x, y, t), e_y(x, y, t))$. The microfluidic device is placed on a translation slider, moving in the opposite direction of the flow, with a velocity tuned as a function of the drop of pressure. The particles remain under the same light, which enhances the quality of the correlation procedure. From these values, we compute the instantaneous shear rate $\dot{\gamma}_i(x, y) = (e_x(x, y, t) - e_x(x, y + dy, t))/(dt * dy)$ and instantaneous velocity field—$v_x(x, y, t) = e_x(x, y, t)/dt$, $v_y(x, y, t) = e_y(x, y, t)/dt$. The mean velocity $V_x(y)$ is obtained by performing the same procedure on rectangular zones of length 300 μm (in the x direction) and width 4.5 μm (in the y direction). This procedure allows us to measure displacement as low as 0.1 μm (using a subpixel fit). In the moving frame, the displacement of the particles is around 5 μm. The systematic error on the velocity is thus around 2%. In the following, error bars will reflect statistical error and correspond to the mean deviation of the measurement.

Measurements are performed in a plane at a sufficient height z; $z = 350$ μm in the vorticity direction above the bottom of the channel, so that the velocity profile is independent of this distance (see the Supplemental Material for Fig. S1 [12]). Under this assumption, our microchannel can be well approximated by two infinite parallel planes: the main streamlines are aligned with the x direction of the channel, along the applied pressure gradient. The local shear stress then depends *linearly* on the position in the y direction: $\sigma(y) = \frac{\Delta P \times y}{L}$, with ΔP the pressure drop, L the channel length, and y the distance from the center of the channel.

Figure 2 displays the velocity profile in the moving frame. As shown in Fig. 2, profiles are merely pluglike, as generally expected for a yield stress fluid. We have also observed that the spatial profiles of the volume fraction across the width of the channel are flat and found as previously [13] that no droplet migration occurs in this geometry. This observation discards the possibility of the spatial variations of the volume fraction as a source of inhomogeneity for this system.

In order to characterize the local dynamical agitation in the system, we focus on the measurement of the standard deviation of the local shear rate $\langle \delta\dot{\gamma}_i(x, y)\rangle$, defined as $\langle \delta\dot{\gamma}_i(x, y)\rangle = \sqrt{\langle \dot{\gamma}_i(x, y)^2\rangle - \langle \dot{\gamma}_i(x, y)\rangle^2}$. In Fig. 3, we represent the spatial profile of $\langle \delta\dot{\gamma}_i\rangle(y)$ for different external forcing. Values are averaged over x along the channel length, at a given position y, and over the time.

A first observation is that, while the maximum fluctuations do occur near the walls, fluctuations are nonvanishing across the whole channel, even for regions close to the center where the local shear stress $\sigma(y)$ becomes less than the macroscopic yield stress Σ_c. Moreover, the values in the center depend upon the forcing but not simply upon the local shear stress. This point is striking and shows that fluidization occurs for shear stress below the macroscopic

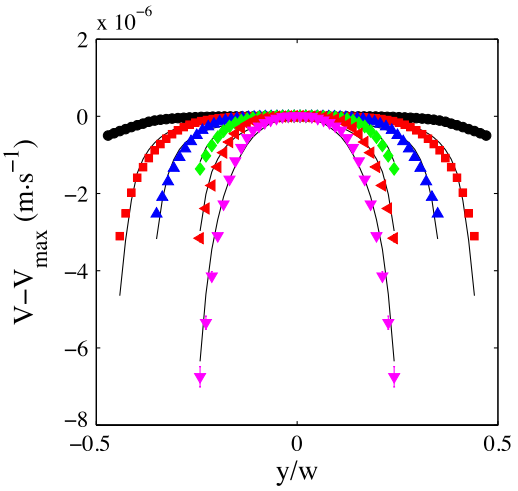

FIG. 2 (color online). Experimental average velocity profiles in the moving frame. From bottom to top, $\Sigma_{max}/\Sigma_c = 2.53, 3.54, 4.55, 6.07, 7.59, 9.10$. The lines correspond to the velocity profiles calculated assuming that the fluidity is proportional to the standard deviation of the strain rate (see text). The error bars correspond to the mean deviation of the measurements (i.e., standard deviation divided by the square root of the measurement number).

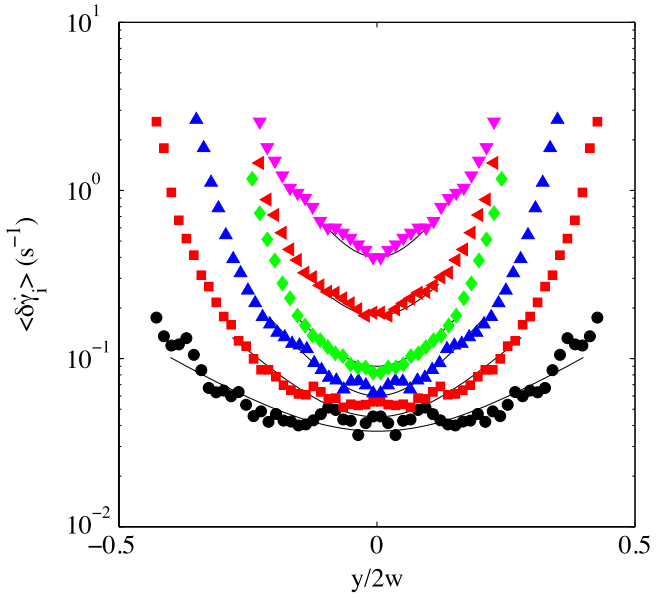

FIG. 3 (color online). Spatial profile of the rms deviation of shear rate, $\langle\delta\dot{\gamma}_i\rangle(y) = \sqrt{\langle\Delta\dot{\gamma}_i^2\rangle(y)}$. The forcing increases from bottom to top, with $\Sigma_{\max}/\Sigma_c = 2.53, 3.54, 4.55, 6.07, 7.59, 9.10$. The lines correspond to hyperbolic cosine functions used to extract the correlation lengths (see text).

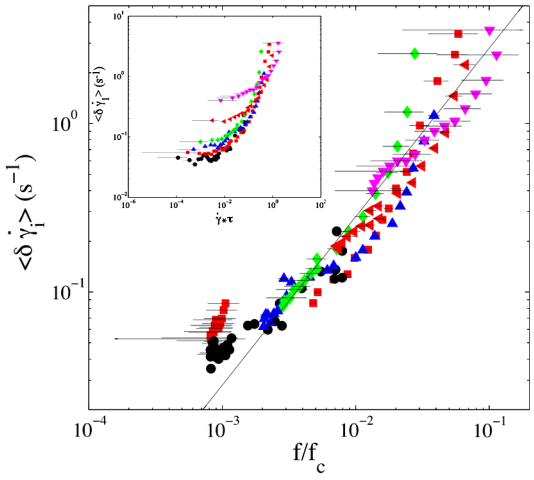

FIG. 4 (color online). Scaling of the local shear-rate rms fluctuation $\langle\delta\dot{\gamma}_i\rangle$ in s^{-1}, with dimensionless fluidity $f(y) = \dot{\gamma}(y)/\sigma(y)$ (same symbols as in Fig. 3). Fluidity is rescaled by $f_c = (\tau\Sigma_c)^{-1}$, using Herschel-Bulkley parameters, measured independently using bulk rheometry. The line corresponds to the linear law $\langle\delta\dot{\gamma}_i\rangle = Af(y)/f_c$, with $A = 29\ s^{-1}$. Inset: $\langle\delta\dot{\gamma}_i\rangle(y)$ in s^{-1} as a function of the mean local shear rate normalized by the characteristic time $\tau = 2.5$ s. Same symbols as in Fig. 3.

yield stress in this geometry, suggesting that the presence of a sheared active region somewhere in the channel modifies the properties of the sample far away from the active region. A similar conclusion was reached for the slow flow of granular materials, where the activated nature of the flow process was evidenced [14]. This also echoes the recent experiment carried out by the Leiden group [15]: in this study, a steel ball resting on a bucket of sand was observed to sink as soon as a shear band was created at the bottom of the bucket, far away from the ball.

To get further insights, we explore the link between the measured velocity fluctuations and the rheological fluidity, as shown in Fig. 3. The local fluidity $f(y)$ is extracted from the knowledge of the local mean shear rate $\dot{\gamma}(y)$ and local shear stress $\sigma(y)$; $f(y) = \dot{\gamma}(y)/\sigma(y)$. The local shear rate $\dot{\gamma}(y)$ is obtained by taking the derivative (finite derivative) of the velocity profiles, and the local shear stress is related to the position in the gap y by the mechanical equilibrium relation $\sigma(y) = \frac{\Delta P}{L} \times y$.

A key finding emerging from this plot is that all data for different external forcing collapse on a *linear master curve*: a linear relation is found between the standard deviation of the local shear rate and the fluidity, $\langle\delta\dot{\gamma}_i\rangle \times (y) \propto f(y)$. In contrast, no such rescaling is found in the plot of the shear-rate rms fluctuations versus the local shear rate; see the inset of Fig. 4, which demonstrates that the fluidity is indeed the relevant physical quantity here and not the local shear rate. To assess further the validity and robustness of the previous scaling law, we use the linear relation between $\langle\delta\dot{\gamma}_i\rangle$ and $f(y)$ in order to rebuild the velocity profiles from the measurements of the fluctuations: using $\langle\delta\dot{\gamma}_i\rangle(y) = Af(y)/f_c$ (with A a numerical prefactor and $f_c = (\tau\Sigma_c)^{-1}$ a characteristic fluidity obtained from the Herschel-Bulkley fit), one expects $V_x(y) - V_x(0) = \int_0^y \frac{f_c}{A}\langle\delta\dot{\gamma}_i\rangle\frac{\Delta P}{L}ydy$. As shown in Fig. 2, the experimental velocity profiles are perfectly captured by this relation. Note that a single fitting parameter A allows us to describe all the profiles which are obtained using the raw data. By using a more monodisperse emulsion [16], we note that the polydispersity of the material does not affect the main result above, i.e., the intimate relationship between fluctuations and fluidity; see the Supplemental Material [12].

These observations show that the extent of fluidization is determined by local shear-rate fluctuations. We note that this result echoes the anomalous scaling of the velocity fluctuations versus shear rate reported for granular materials [17]. In these systems, the velocity fluctuations are often considered to be one of the measures of an effective *granular temperature* [17], and, for simulations of sheared soft disks at finite temperatures [18], a similar link between effective temperature and viscosity has been observed.

With these measurements, we are able for the first time to directly connect the microscopic to the macroscopic rheological behavior. The standard deviation of the local shear rate is local information, but the movement of a droplet can promote another one in its vicinity. To characterize the flow heterogeneity, we explore the spatial variation of these motions. In a first step, we consider the decay length ξ_v of the shear-rate fluctuation profile,

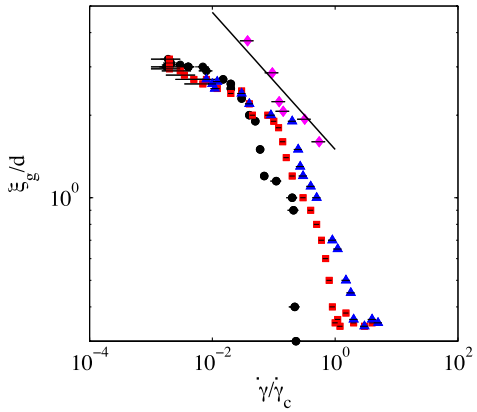

FIG. 5 (color online). Variation of extracted correlation lengths normalized by the diameter d of a droplet as a function of the local shear rate, rescaled with $\dot{\gamma}_c$. The $\diamond$ symbols correspond to ξ_v, calculated from the rms strain-rate profiles, $\langle\dot{\delta}\gamma_i\rangle$. Other symbols are the decay length of the velocity correlation function, $G_y(x, y)$, along the flow direction x for a given strain rate $\dot{\gamma}(y)$, obtained for different applied forcings ($\bigcirc$'s correspond to $\Sigma_{\max}/\Sigma_c = 2.53$, $\square$'s to 3.54, and $\triangle$'s to 4.55). The solid line corresponds to a power-law scaling with an exponent equal to -0.25.

$\langle\dot{\delta}\gamma_i\rangle(y)$, as in Fig. 3. To quantify further this behavior, the central part of the profile is fitted by a hyperbolic cosine function $\cosh(y/\xi)$, from which the decay length ξ is extracted. This fitting model for $\langle\dot{\delta}\gamma_i\rangle(y)$ is actually inspired by our previous work [5,8], where fluidity was shown to obey a nonlocal equation $\xi^2 \frac{\partial^2 f}{\partial^2 y} + f - f_b(\sigma) = 0$; ξ is the cooperativity length, and $f_b(\sigma)$ is the fluidity in wide geometry under constant shear stress and thus vanishes for stresses lower than the yield stress Σ_c, i.e., close to the center of the slab. As $\langle\dot{\delta}\gamma_i\rangle(y)$ is found to be proportional to the fluidity—see Fig. 4—we assume that, for stress smaller than the yield stress, it follows that $\xi_v^2 \frac{\partial^2\langle\delta\dot{\gamma}_i\rangle}{\partial^2 y} + \langle\delta\dot{\gamma}_i\rangle = 0$. As shown in Fig. 2, this equation provides a very good fit for the experimental data for the shear-rate fluctuation profile $\langle\dot{\delta}\gamma_i\rangle(y)$ for $\sigma(y) < 2\Sigma_c$. In Fig. 5, the results for ξ_v are plotted as a function of the mean shear rate $\dot{\gamma}$, calculated by averaging the local shear rate $\dot{\gamma}(y)$ over the space in the fitted zone [i.e., for y, verifying $\sigma(y) < 2\Sigma_c$]. The correlation length is shown to increase as the shear rate decreases. In Ref. [8], we predicted a power-law divergence for the fluidity correlation length in the form $\xi \sim \dot{\gamma}^{-\alpha}$, with $\alpha = 1/4$. The results in Fig. 5 confirm a similar slow increase of the correlation length as the shear rate goes to zero, and this predicted power-law divergence gives a fair description of this diverging behavior.

In a second step, we considered an alternative correlation length in the material, by measuring the nonaffine velocity correlation function $G_y(x, y) = \langle v_y(0, y) v_y(x, y)\rangle_t$, where $\langle\rangle_t$ implies a temporal average; $v_y(x, y)$ is the instantaneous velocity map. In a Poiseuille flow, the local strain rate, $\dot{\gamma}(y)$, depends on the distance y from the center of the channel, and this allowed us to explore the decay length of $G_y(x, y)$ along x for a given shear rate $\dot{\gamma}(y)$. A correlation length, ξ_g, is accordingly extracted from the spatial decay of $G_y(x, \dot{\gamma})$ [using the criteria $G_y(x = \xi_g) = e^{-1}$]. In Fig. 5, we show the variation of ξ_g with $\dot{\gamma}$, collecting data for different external forcings. A key feature of this plot is that we observe a collapse of the data points on a master curve for various imposed forcings, in a strain-rate window spanning over more than two decades. Furthermore, this figure shows that the correlations again significantly increase as $\dot{\gamma}$ decreases. Although ξ_g differs from the previously defined lengths (ξ and ξ_v), this result suggests the increase of cooperativity close to yielding. The extracted length scale grows roughly logarithmic with shear rate or as with a power law with a small exponent. This result echoes the results on soft spheres where an exponent of -0.3 was observed [19].

In conclusion, we have demonstrated the link between macroscopic forcing and the local dynamical fluctuations in the form of a scaling relationship between fluidity and velocity fluctuations. Moreover, we observe correlations among these local fluctuations, with the measured correlation length scale increasing with decreasing strain rates, as predicted by theoretical models. The mechanical noise induced by the flow itself is the source of nonlocality. The occurrence of cooperativity in the rheological properties in the jammed regime echoes the recent evidence for a nonlocal anomalous behavior of the viscosity in the supercooled regime, furthermore in direct connection to dynamic heterogeneities [20].

We acknowledge funding from ANR SYSCOM and GIS Matériaux en Aquitaine.

[1] C. A. Angell, Science **267**, 1924 (1995).
[2] P. Coussot, Soft Matter **3**, 528 (2007).
[3] D. Bonn and M. M. Denn, Science **324**, 1401 (2009).
[4] L. Isa, R. Besseling, and W. C. K. Poon, Phys. Rev. Lett. **98**, 198305 (2007); P. Schall, D. A. Weitz, and F. Spaepen, Science **318**, 1895 (2007); G. Ovarlez, Q. Barral, and P. Coussot, Nature Mater. **9**, 115 (2010); T. Divoux, D. Tamarii, C. Barentin, and S. Manneville, Phys. Rev. Lett. **104**, 208301 (2010); K. N. Nordstrom, E. Verneuil, P. E Arratia, A. Basu, Z. Zhang, A. G. Yodh, J. P. Gollub, and D. J. Durian, *ibid.* **105**, 175701 (2010).
[5] J. Goyon, A. Colin, G. Ovarlez, A. Ajdari, and L. Bocquet, Nature (London) **454**, 84 (2008).
[6] P. Olsson and S. Teitel, Phys. Rev. Lett. **99**, 178001 (2007); A. Furukawa and H. Tanaka, Nature Mater. **8**, 601 (2009); A. Lemaître and C. Caroli, Phys. Rev. Lett. **103**, 065501 (2009); H. G. E. Hentschel, S. Karmakar, E. Lerner, and I. Procaccia, *ibid.* **104**, 025501 (2010).

[7] C. Heussinger and J.-L. Barrat, Phys. Rev. Lett. **102**, 218303 (2009).
[8] L. Bocquet, A. Colin, and A. Ajdari, Phys. Rev. Lett. **103**, 036001 (2009).
[9] B. P. Tighe, E. Woldhuis, J. J. C. Remmers, W. van Saarloos, and M. van Hecke, Phys. Rev. Lett. **105**, 088303 (2010).
[10] O. Pouliquen and Y. Forterre, Phil. Trans. R. Soc. A **367**, 5091 (2009).
[11] P. Guillot, P. Panizza, J. B. Salmon, M. Joanicot, A. Colin, C. H. Bruneau, and T. Colin, Langmuir **22**, 6438 (2006).
[12] See Supplemental Material at http://link.aps.org/supplemental/10.1103/PhysRevLett.108.148301 for details about the z dependence of the velocity profiles.
[13] G. Ovarlez, S. Rodts, A. Ragouilliaux, P. Coussot, J. Goyon, and A. Colin, Phys. Rev. E **78**, 036307 (2008).
[14] K. A. Reddy, Y. Forterre, and O. Pouliquen, Phys. Rev. Lett. **106**, 108301 (2011).
[15] K. Nichol, A. Zanin, R. Bastien, E. Wandersman, and M. van Hecke, Phys. Rev. Lett. **104**, 078302 (2010).
[16] T. G. Mason and J. Bibette, Phys. Rev. Lett. **77**, 3481 (1996); C. Mabille, F. Leal Calderon, J. Bibette, and V. Schmitt, Europhys. Lett. **61**, 708 (2003).
[17] W. Losert, L. Bocquet, T. C. Lubensky, and J. P. Gollub, Phys. Rev. Lett. **85**, 1428 (2000); C. M. Song, P. Wang, and H. A. Makse, Proc. Natl. Acad. Sci. U.S.A. **102**, 2299 (2005).
[18] T. K. Haxton and A. J. Liu, Phys. Rev. Lett. **99**, 195701 (2007).
[19] K. N. Nordstrom, J. P. Gollub, and D. J. Durian, Phys. Rev. E **84**, 021403 (2011).
[20] A. Furukawa and H. Tanaka, Phys. Rev. Lett. **103**, 135703 (2009).